CO2 absorption into a polymer within a multilayer structure, the case of EVA in photovoltaic modules

Axel Briand, Antoine Leybros, Claire Audoin, Jean Christophe Ruiz, Fabrice Lamadie, Agnès Grandjean

CO_2 absorption into a polymer within a multilayer structure, the case of EVA in photovoltaic modules

Axel Briand[1,2], Antoine Leybros[1], Claire Audoin[2], Jean Christophe Ruiz[1], Fabrice Lamadie[1], Agnès Grandjean[1]

1- CEA, DES, ISEC, DMRC, Univ Montpellier, Marcoule, France

2- Univ Grenoble Alpes, CEA, DRT, LITEN, DTS, INES, F-38 000 Grenoble, France.

Abstract

In the objective to develop an efficient circular economy with a low environmental impact in the photovoltaic field, the supercritical CO_2 delamination of photovoltaic modules is an interesting alternative way. This paper describes the first phase of this process: the CO_2 absorption into poly(ethylene-co-vinyl acetate) (EVA-28) in the photovoltaic multilayer structure. The melting temperature of EVA-28 in CO_2 medium was determined by high-pressure differential scanning calorimetry for pressures ranging from atmospheric pressure to 150 bar. This thermodynamic phase equilibrium of the mixture EVA-28/CO_2 was determined by the Sanchez-Lacombe EoS modified to take into account the crystallinity and the cross-linking of the polymer. This model was applied with great agreement to swelling experiments for pressures ranging from 60 to 200 bar at temperatures of 60, 75 and 90°C. The diffusion coefficient of CO_2 into EVA-28 was determined in the same conditions ranging at 130 bar, from 4 $x10^{-9}$ $m^2.s^{-1}$ (60°C) to $7x10^{-9}$ $m^2.s^{-1}$ (90°C). The impact of different interfaces of photovoltaic modules on the CO_2 diffusivity into the EVA-28 was studied by an original method of apparent length of diffusion post treatment. This experiment demonstrated a preferential diffusion at the rear side of the cell interface due to an important porosity and at the "backsheet" interface due to favourable interactions.

1. Introduction

The increase in demand of energy all around the world coupled to the willingness to develop renewable energy production generate an important growth of the electrical energy production from solar sources using photovoltaic panels (PV) since the early 2000s. This growth is expected to continue and estimated to reach between 7,6 and 22 TWp of installed PV in 2050 [1]. The first generation of photovoltaic panels installed are now coming to the end of their life. The cumulative mass of end-of-life PV panels worldwide is expected to reach between 2 and 8 million tonnes by 2030 [2]. In this context of growth in energy demand using solar energy and with a view to a circular economy to recover valuable materials, it becomes more than necessary to develop efficient, cost-effective and eco-friendly recycling processes. Installed PV panels are mostly based on crystalline silicon PV cells. Until 2016, more than 80% of installed PV panels were based on the Si-Al-BSF cell technology [3]. However, cell technologies evolve very rapidly meaning that the recycling techniques must be versatile to adapt to new technologies developed.

A crystalline silicon-based photovoltaic panel is defined as the assembly of the photovoltaic module stiffened by an aluminium frame and managed electrically by a junction box. PV module structure consists of a set of electrically connected crystalline silicon-based cells encapsulated in an encapsulating polymer between a glass front face and a rear face in polymer sheet ("backsheet") (Figure 1). In more than 90% of PV panels, in 2019 [1], encapsulating polymer used was the EVA - poly(ethylene-co-vinyl acetate). The "backsheet" is a multilayer assembly of polymers. It generally consists of a polyethylene terephthalate (PET) layer in adhesion between two layers of fluoropolymer such as polyvinyl fluoride (PVF).

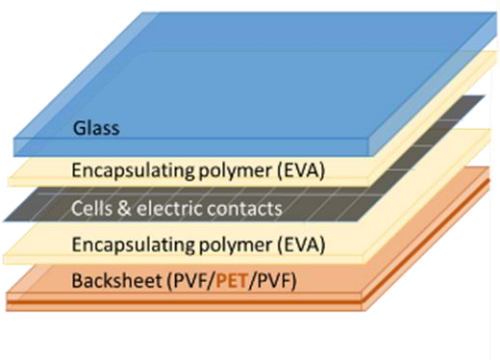

Figure 1: Photovoltaic module's constitution

Technologies developed to recycle these modules consists on multi-stage processes [4]:

(1) First a pre-treatment to remove the aluminium structure and the junction box,
(2) A coupling of thermal [5], [6], chemical [7]–[9] or mechanical [10] routes to delaminate the multi-layer structure (silicon cell/glass/backsheet/EVA) and
(3) A specific chemical treatment to extract the valuable metals (Ag, In, Si…) from the silicon cell [11]–[14] or to recycle silicon [15].

The use of chemical processes for the delamination step (2) need organic solvents, to dissolve EVA (mainly in temperature or coupled with ultrasound or mechanical stirring). These solvent are difficult to recycle and moreover, the reaction time is relatively long (>1h for pieces with a width of 3cm) [7]. Thermal treatments at high temperature (≥500°C) to decompose EVA to separate glass and cell requires a long residence time (>3h for pieces of 5x5cm^2) to allow decomposition of EVA inside the module [6]. In addition, the decomposition of polymers generates toxic gaseous compounds (HF from "backsheet" and CO) requiring a complex step of gaseous post-treatment [5]. The gaseous effluents considerably impact the life-cycle analysis of the global recycling process [4]. The mechanical treatments are generally poorly selective for the material separation and generate a loss of valuable materials like silver or indium [10]. For an efficient circular economy with a low environmental impact, we propose the use of supercritical CO_2 (SC-CO_2) based process as an alternative way for recycling end-of-life photovoltaic panels.

The delamination in SC-CO_2 of PV modules, consists on separating the different layers of the structure, layer by layer, without breaking the glass and contaminated the valuable materials. The study of the delamination of photovoltaic modules in a SC-CO_2 medium focuses on the separation of the EVA encapsulant from the various components to which it adheres. The process consists on a phase of CO_2 absorption within the polymer at a pressure above the critical pressure followed by a rapid depressurization (from 1 bar.s^{-1} to 300 bar.s^{-1}) leading to the foaming of the EVA. As observed for other polymers, this foaming phenomenon leads to a loss of adhesion at the interfaces of the foamed polymer [16], or even delamination [17].

This paper focuses on the first phase of the SC-CO_2 delamination: the CO_2 absorption into the EVA in photovoltaic modules. The CO_2 absorption into polymers is widely described in the literature [18]–[21]. The specific case of EVA was studied by Shieh and Lin [22] for different grades, i.e. for different percentages by weight of vinyl acetate group in the polymer constitution, EVA-16, EVA-18, EVA-25 and EVA-28 between 25°C and 52°C until to 340 bar and by Jacobs & al. [23] for EVA-40 between 50°C and 75°C until to 250 bar. However, the CO_2 absorption into a polymer in a multilayer structure is not described. For a gas absorption into a polymer two aspects are basically considered: the phase equilibrium of CO_2/polymer (solubility) and the kinetic absorption of CO_2 into the EVA (diffusion coefficient). In this study, we consider also the role of interfaces that impacts the absorption of CO_2 into the polymer.

2. Experimental

2.1. Materials

The EVA used in this study is an EVA-28 from STRE. This copolymer is made by radical polymerisation and shaped in the form of films (600µm in this work) containing cross-linking agents (peroxides) for use by hot lamination (> 120°C) in photovoltaic modules. EVA is in its native state a semi-crystalline rubbery polymer at ambient temperature ($T_a > T_g$). The constituent units derived from ethylene tend to organise themselves and form crystalline phases. On the contrary, the constituent units derived from vinyl acetate, due to their steric hindrance, tend to limit the organisation of macromolecules. The cross-linking agents are activated during the PV module assembly process and enable the formation of a three-dimensional network, i.e. cross-linking, through the formation of covalent bonds between the EVA macromolecules. Therefore, EVA within PV modules is a semi-crystalline cross-linked rubbery polymer. The characteristics of the EVA-28 used in this work were determined in a previous work [24] and are summarized in Table 1.

Grade	% VA (massic)	% VA (molar)	T_g (°C)	T_m (°C)	X_c (%)	M_n (kg.mol^{-1})
EVA 28	27,5	10,8	-37	75	17	35

Table 1:EVA characteristics (data from [24])

The backsheet used is constituted as follows: PVF/PET/PVF. The glass used is borosilicated and has a thickness of 3mm. PV cells used in this work are based on Si-Al-BSF technology and have a thickness of 200µm.

Carbon dioxide (> 99.99% purity) was provided from Air Liquide.

2.2. Determination of EVA's melting temperature in function of CO_2 pressure

The melting temperature of EVA in function of CO_2 pressure was determined by using a HP-DSC (Sensys Evo, Setaram) for in-situ measurement with high-pressure crucibles. The schematic of this system is shown in Figure 1. The gas pressure was increased to the required level using an ISCO 260D syringe pump.

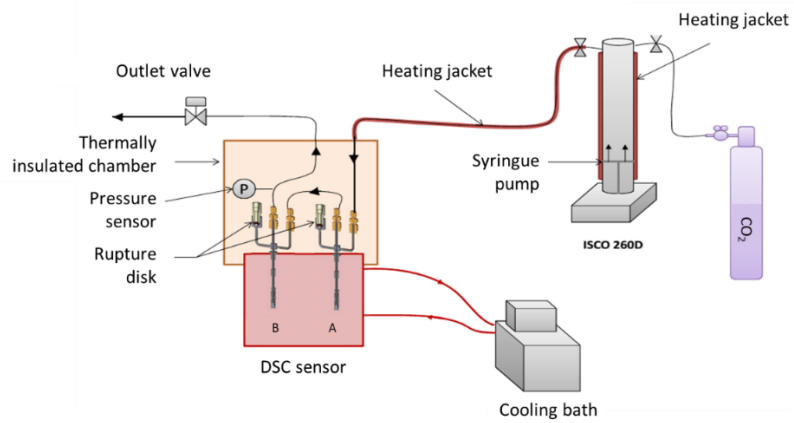

Figure 2: Scheme of HP-DSC set-up - A is the reference crucible and B the measurement crucible

The procedure described by Huang & al. [25], applied to measure melting and glass transition temperatures for various polymers (PLA, PS, iPP and PC) under CO_2 pressure, was used here for EVA-28. The samples mass used were weighted of about 10 mg.

2.3. *Swelling experiments*

This technique consists on following in-situ the volume variation of a polymer during the CO_2 absorption. The swelling of the sample $(\Delta V/V_0)$ is related to the volume fraction of CO_2 within the polymer $(\emptyset_1)$ or can be seen as the CO_2 solubility in the polymer (in mol/mol) (1).

$$\frac{\Delta V}{V_0} = \frac{\emptyset_1}{1-\emptyset_1} \quad (1)$$

This method requires the use of a high-pressure cell composed of transparent sapphire windows allowing the measurement of the dimensional variation of the surface or thickness of a sample, using a camera [26]. The setup used for swelling experiments is shown in Figure 3. The CO_2 was supplied thanks to a CO_2 bottle connected to a high-pressure pump (Pump HPP400-B from SFE process) equipped with a pressure regulation system and connected to a chiller (PCNO21.01-NED from National Lab). The pump has a maximum operating flow rate of 50 g.min^{-1}. The operating flow rate was set at 20 g.min^{-1} for pressure transients. The CO_2 was heated up before entering in the visualization cell thanks to a heat exchanger.

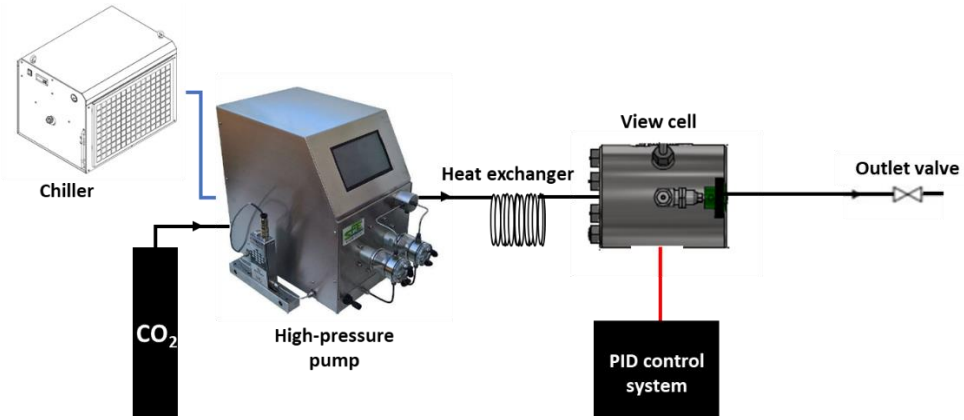

Figure 3: Scheme of the experimental setup used for swelling experiments

EVA samples were loaded in advance into the high-pressure cell (A085FR from SFE Process) with a volume of 74 mL (Figure 4.(a)) in which they are contacting with supercritical CO_2. The cell has a maximum operating pressure of 300 bar and a maximum operating temperature of 100°C. The cell is equipped with four heating rods, two thermocouples of type K (one in the cell shell and one in the cell) and one pressure transducer. They are all connected to a PID control system (nanodac) for temperature control.

The optical set-up (Figure 4.(b)) designed to measure swelling is a backlight set-up in which the visualization cell is placed between the camera and the lighting. The lighting used is a 150x40mm LED panel (long lasting ultra-bright backlight from Phlox) with a luminance of 18,000 cd/m^2 and an uniformity > 95%, ensuring an homogeneous illumination of the entire sample. Opposite, a color camera (Thorlabs, 1280x1024 square pixels of 3.60 µm on a side) associated with a high magnification lens (Keyence standard zoom lens, magnification x20 to x200) allows the acquisition of images.

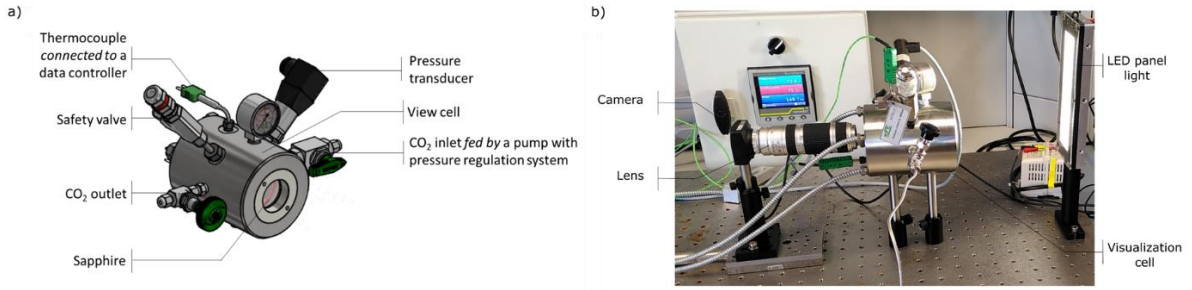

Figure 4: (a) The schematic diagram of the high-pressure cell and (b) a photography of the optical set-up designed for swelling experiments

Each series of measurements corresponds to the acquisition of an EVA swelling cycle for considering an isotherm and a pressure evolution (Figure 5 (b)) in 15 minutes steps. Swelling process lasted up to 1,5h for all experiments. The acquisitions were performed at a variable frequency of 10 frames per second (fps) during pressure transients and 0,2 fps during pressure stages. The image processing is relatively simple and is based on 3 steps. The images are first transformed into a binary image and thresholded with respect to a background level calculated from the average light intensity measured in a 50x50 pixels square in the top left corner of the image (Figure 5.(a)). Six transversal profiles (y=cste), regularly positioned along the x-axis as shown in Figure 5.(a), are then extracted from the binarized image. On each of these profiles the non-zero pixels are finally counted to measure the thickness of the sample on the considered profile. The image processing process is fully automated and allows the processing of one acquisition (~4700 images) in 5 minutes on a standard computing machine (Intel Core i7 at 2.60 GHz, 16 GB ram).

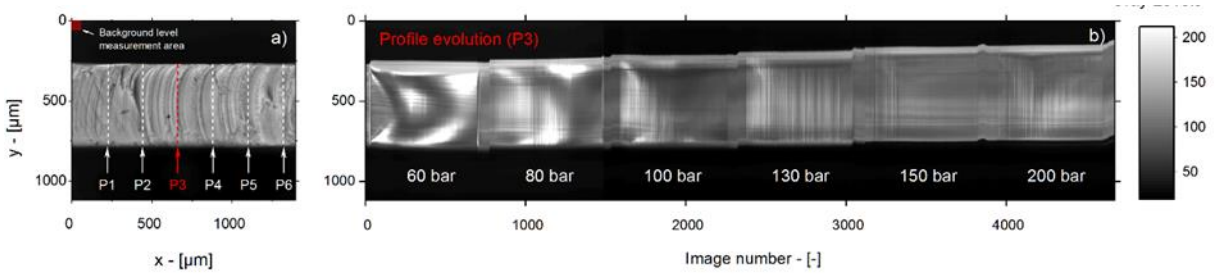

Figure 5: (a) Edge view of the EVA and (b) example of the evolution of the profile P3 (red profile on (a)) over the course of the experience)

The six profiles measured by image processing are averaged and the measurements are repeated three times per isotherm experiment in order to calculate a standard deviation. The equilibrium swelling is calculated from the average of the last 10 images of the pressure stage.

2.4. Sanchez-Lacombe equation of state

The Equation of State (EoS) given by Sanchez-Lacombe [27] (2) is one of the most widely used equations to determine the phase equilibrium of a polymer/fluid mixture. This EoS allows to predict the absorption of a fluid into a polymer according to pressure and temperature conditions using three intrinsic parameters of polymer, without free parameters. This EoS is valid for liquid polymers of high molecular weight (> 8 000 g.mol^{-1}) meaning that the solubility of the polymer in the fluid can be assumed to be equal to zero. However, this is also valid for solid amorphous polymers when the working temperature is higher than the glass transition temperature (T_g) [28]. To determine this EoS, Sanchez and Lacombe introduce the concept of free volume inside the polymer structure [27]. This EoS is the following:

$$\widehat{\rho^2} + \hat{P}_i + \hat{T}_i\left[\ln(1-\hat{\rho}) + \left(1 - {}^1\!/_r\right)\hat{\rho}\right] = 0 \qquad (2)$$

Where $\hat{\rho}$ is the ratio of occupied sites; $\hat{P}_i = {}^{P}/_{P_i^*}$ and $\hat{T}_i = {}^{T}/_{T_i^*}$ respectively the reduce pressure and reduce temperature. Where P_i^* and T_i^* corresponds respectively to a characteristic pressure and temperature of the studied compounds (Table 2), and P and T respectively the studied pressure and temperature; and $r = \frac{M_n P^*}{kT^*\rho^*}$ refers to the number of occupied sites where M_n corresponds to the molecular weight of the compounds (kg.mol^{-1}) and ρ* the density of the compounds (kg.m^{-3}).

Thus, each compound, fluid and polymer, can be entirely defined from only three characteristic parameters (P_i *, T_i *, ρ *). Table 2 reports the values of these parameters for CO_2 [29] and EVA. Here we calculated these parameters for EVA-28 (28%wt EVA) by interpolation from SL parameters defined for PEHD (0%wt VA) [27], EVA-40 (40%wt VA) [23] and PVAc (100%wt VA) [27] thanks to the density (ρ*) of each of the polymers.

Parameter	Carbon dioxide [29]	EVA-28
M (kg.mol^{-1})	0,044	35
T_i* (K)	300	635
P_i* (MPa)	650	460
ρ* (kg.m^{-3})	1515	945

Table 2: Sanchez-Lacombe parameters

Cross-linking induces intermolecular covalent bonds that limit the absorption of a fluid into a polymer. Thus, it must be considered in the thermodynamic model that EVA encapsulant of photovoltaic modules are cross-linked polymers. The modified Sanchez-Lacombe model allows to take into account the cross-linking of a polymer [30]. It integrates a cross-linking factor (f) which depends on the molecular weight between 2 cross-linking nodes (M_e) and takes into account the volume variation linked to the cross-linking (α_s) (4).

$$f = \frac{1}{M_e}\left(1 - \frac{2M_e}{M_n}\right) \tag{3}$$

Where M_n is the molecular weight of the polymer (kg.mol^{-1}).

Thus, the modified Sanchez-Lacombe EoS (2) for the cross-linked polymer/fluid mixture (4) is the following:

$$\widehat{\rho^2} + \hat{P} + \hat{T}\left[\ln(1-\hat{\rho}) + \left(1 - \frac{\emptyset_1}{r_1}\right)\hat{\rho} + \frac{\emptyset_2}{r_2}\hat{\rho}\left(\alpha_s^2 - \frac{2}{f}\right)\right] = 0 \tag{4}$$

Where $\emptyset_1$ as already described corresponds to the volume fraction of the fluid (CO_2) and $\emptyset_2 = 1 - \emptyset_1$ the volume fraction of the polymer (EVA); r_1 and r_2 refer to the number of sites occupied respectively by the fluid and the polymer. $\hat{P} = {}^{P}/_{P^*}$ with P* the characteristic pressure of the mixture composed of the fluid and the polymer calculated from the characteristic pressure of pure compounds, the volume fraction of each compounds and k_{ij} (6), an adimensional binary interaction parameter to evaluate the deviation from ideality. It is usually evaluated as a function of temperature.

$$P^* = \emptyset_1 P_1^* + \emptyset_2 P_2^* + \emptyset_1\emptyset_2 (P_1^* P_2^*)^{1/2}\left(1 - k_{ij}\right) \tag{5}$$

In addition, EVA is a semi-crystalline polymer of low crystallinity (X_C=0.17). The mechanical effect of the crystalline phases can be assimilated to that of a cross-linking network. The crystalline phases can be considered impermeable to the penetrating species. Thus, the CO_2 solubility (mol.mol^{-1}) within the semi-crystalline polymer ($\emptyset_{sc}$) can be corrected from the weight percentage of crystalline phases (X) and the CO_2 solubility within the polymer in its amorphous phase ($\emptyset_{am}$) (6) [31].

$$\emptyset_{sc} = (1 - X)\emptyset_{am} \quad (6)$$

Where $\emptyset_{am} \equiv \emptyset_1$, previously introduced.

2.5. Diffusion coefficient

The mathematical theory of diffusion proposed by Fick in 1855 is based on the hypothesis that the rate of transfer of the diffusing substance across the unit area of a section (F) is proportional to the concentration (C) gradient -measured normally with respect to the section (7).

$$F(t) = -D\frac{\partial C}{\partial x} \quad (7)$$

Where D refers to the diffusion coefficient ($m^2.s^{-1}$)

Crank solves the diffusion equations proposed by Fick for different geometric forms and boundary conditions [32]. These solutions allow the determination of the diffusion coefficient, in particular through experimental monitoring of the mass of the system under study. For a sample with a "flat sheet" type geometrical shape, and with an uniform initial pressure at the surfaces, the mass of fluid absorbed within the polymer at time t (M_t in kg) is expressed as a function of time (t in s), of the diffusion coefficient (D in $m^2.s^{-1}$) and of the thickness of the sample (l in m) (8).

$$\frac{M_t}{M_\infty} = 1 - \sum_{n=0}^{\infty} \frac{8}{(2n+1)^2\pi^2} exp(-D(2n+1)^2\pi^2 t/4l^2) \quad (8)$$

Where M_∞ corresponds to the weight saving of the polymer at equilibrium

To determine by volumetric measurement the diffusion coefficient, we assume that the solubility of the polymer in CO_2 is null. Thus, it is possible to relate the variation in volume to the variation in mass (9) and to use mathematical solutions to the diffusion equations [26].

$$\frac{V_t - V_0}{V_\infty - V_0} = \frac{M_t}{M_\infty} \quad (9)$$

2.6. Interface diffusion experiments

It is possible to determine an interface diffusion coefficient (D_{int} in $m^2.s^{-1}$) depending on the nature of the interfaces between the polymer and another materials of the photovoltaic module. Indeed assuming a Fickian diffusion, the diffusion length of the CO_2 at the interface (L in meter) is proportional to the square root of the time (t in second) multiply by the "interface" diffusion coefficient (D_{int} in $m^2.s^{-1}$) *(10)*.

$$L \propto D_{int}\sqrt{t} \quad (10)$$

For this purpose, various samples were produced to study each of the interfaces isolated. The structure is as follows: material studied/EVA/material studied. The materials respectively studied were the glass, the front side of the cell, the rear side of the cell and the "backsheet". These samples were treated with supercritical CO_2 with different contacting time. The length of diffusion is apparent thanks to the foaming caused by the rapid and always identical depressurisation carried out at the end of the treatment.

By carrying out different contacting times for each of the interfaces, it is possible to measure the interface diffusion length (red arrow in Figure 6), by measuring the length between the edge of the structure and the bubble front (diffusion front), to determine the interface diffusion coefficient (D_{int}) for each of the interfaces (11).

$$L^2 = D_{int}t + b_0 \quad (11)$$

Where b_0 is a constant determined experimentally for each interface.

An example of the method is shown in Figure 6 for backsheet/EVA/backsheet samples.

Figure 6: Interface advance of the front of diffusion over time (example for backsheet/EVA/backsheet samples)

2.7. Scanning electron microscopy

The morphology of the rear side of the cell was determined with a Scanning Electron Microscope FEI Inspect S50 equipped with Bruker Nano Quantax EDS detector.

3. Results and discussion

Firstly, the melting properties of EVA under CO_2 pressure will be presented. This characterization enables to describe precisely, thanks to SL EoS correlated to swelling experiments, the phase equilibrium CO_2/EVA in function of pressure and temperature by distinguishing the behaviour before melting start, in the melting range and after melting end. Then, the diffusivity of CO_2 into EVA measured by swelling experiments will be presented in function of pressure and temperature. After characterizing the CO_2 absorption into EVA alone, the influence of the different PV module interfaces will be presented in the aim to define which interfaces are kinetically limiting or favourable.

3.1. EVA's melting under CO_2 pressure

As described in paragraph 2.1, the EVA used for solar applications is cross-linked and semi-crystalline. The presence of crystalline or non-crystalline phases, considered at first sight to be impermeable to CO_2, modifies the absorption of CO_2 within the polymer. In addition, the temperature range at which photovoltaic modules are treated with SC-CO_2 (60-90°C) contains the melting range of EVA-28 at atmospheric pressure (70-80°C). Moreover, CO_2 can lower the melting temperature of polymers [25]. Therefore, it is necessary to know the melting range of EVA under CO_2 pressure. Figure 7 identifies the melting start, the melting peak and the melting end. The melting peak of EVA is slightly lowered in the presence of CO_2 (between 1°C and 5°C). Moreover under CO_2 the melting zone is reduced, i.e. the melting start temperature is slightly increased (about 5°C) while the melting end temperature is more significantly lowered, by about 7°C (from 85°C to 78°C) from 60 bar. These measurements are similar to those performed on EVA-25 samples by Sarver et al [33]. The results from DSC measurements, during the heating phase at 10°C.min^{-1}, are summarised in Figure 7 in the form of a pressure/temperature phase diagram of the EVA.

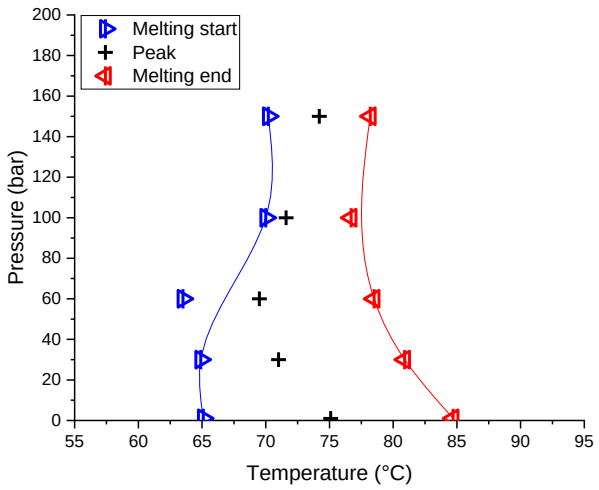

Figure 7: Phase diagram of EVA under CO_2 pressure

According to these results, we can conclude that EVA in the presence of CO_2 at a pressure above 60 bar is semi-crystalline with a crystallinity rate of 17% (X_c=0.17) below 68°C and amorphous (X_c=0) from 78°C onwards. Within the melting range, a partial melting of the crystalline phases is considered, which results in an intermediate degree of crystallinity.

3.2. *CO_2 absorption into EVA at equilibrium - Solubility*

The CO_2 absorption into EVA at equilibrium was determined by means of swelling measurements (paragraph 2.3). The equilibrium swelling of the EVA was determined as a function of CO_2 pressure and temperature. These experimental measurements are compared with the results obtained from the Sanchez-Lacombe equation of state. Figure 8 shows the results of swelling as a function of pressure obtained for measurements outside the melting range (below at 60°C and above at 90°C). Results of the modelling (from the SL EoS) are also shown on this figure.

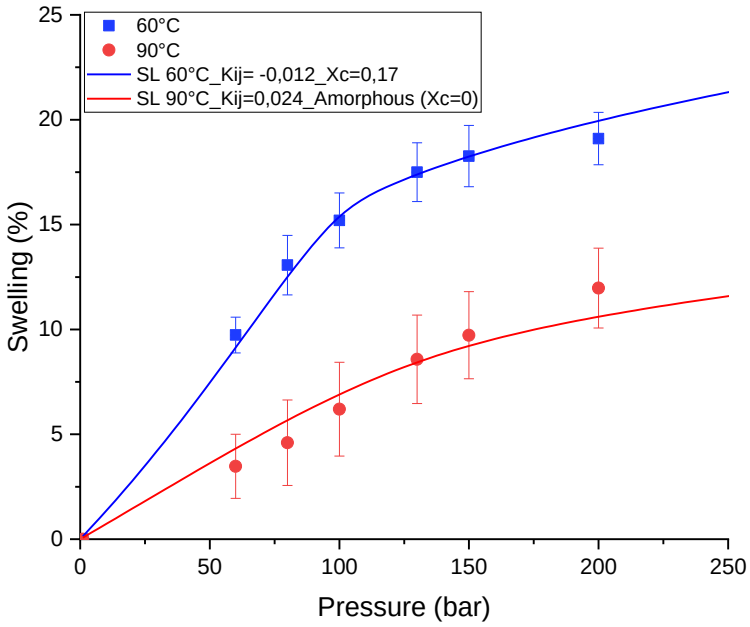

Figure 8: Swelling measurements and Sanchez Lacombe EoS fit at 60°C (below T_m) and 90°C (above T_m) and line obtained by calculation using SL EoS

The binary interaction parameter (K_{ij}) changes as a function of temperature (-0.012 to 60°C and 0.024 to 90°C). This has been adjusted by minimising the average absolute rate deviation (AARD%) (Table 3). Determination of the binary interaction parameters at 60°C and 90°C made it possible to set the binary interaction parameter at 75°C by linear regression (12).

$$K_{ij} = 0{,}0012\mathrm{T} - 0{,}0833 \qquad (12)$$

With T the temperature (°C).

At 60°C, the equilibrium swelling increases significantly up to 100 bar before increasing more slowly thereafter. The equilibrium swelling at 60°C is approximately twice as high as at 90°C for all measurements. Figure 9 shows the results obtained for measurements performed at 75°C, i.e. within the melting range of EVA-28.

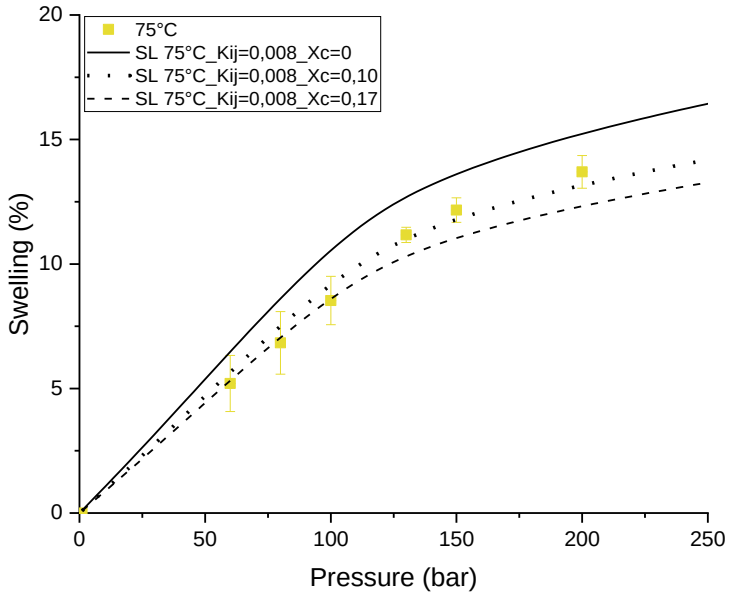

Figure 9: Swelling measurements (+) and Sanchez-Lacombe EoS fit for different crystallinities (Xc=0 – amorphous; 0,10 and 0,17)

For 75°C, different calculations based on the SL EoS were made for different crystallinities (X_c=0; 0.10 and 0.17). The measurements made are closer to the curve plotted for X_c=0.10 with an AARD of 5.5%. Table 3 summarized the SL parameters and the AARD for the different temperatures.

Temperature (°C)	K_{ij}	X_c	AARD (%)
60	-0,012	0,17	2,9
75	0,008	0,10	5,5
90	0,024	0	11,5

Table 3 : The crystallinity (Xc), the SL binary interaction parameters (K_{ij}) and the average absolute rate deviation (AARD) from the SL EoS

The results of swellings at equilibrium are much lower (about half as much) than those of Jacobs & al. [23] obtained with an EVA-40. Firstly, this difference can be explained by the difference of EVA used EVA-28 here and EVA-40 in Jacobs et al., meaning a difference of crystallinity. Indeed, when the mass fraction of vinyl acetate is increased the crystallinity decreases [24]. Therefore, the EVA-28 is more crystalline than the EVA-40 and has less area to solubilise CO_2, leading to a lower swelling. This effect has been well described by Shieh and Lin for different EVA with different VA ratio [22]. Moreover, the polymer used by Jacobs & al. was uncrosslinked while cross-linking limits swelling.

After having fitted the binary interaction parameters (K_{ij}) and the degree of crystallinity (X_c) by validation with swelling measurements, SL EoS allows to give relevant information for process operating parameters definition and sizing. Especially this modelling can predict the quantity of CO_2 absorbed in the polymer which is an important information to describe the EVA foaming with the aim to delaminate a PV module. As an example, Figure 10 shows the calculation of the variation of mass fraction of CO_2 absorbed at equilibrium into EVA in function of pressure and temperature.

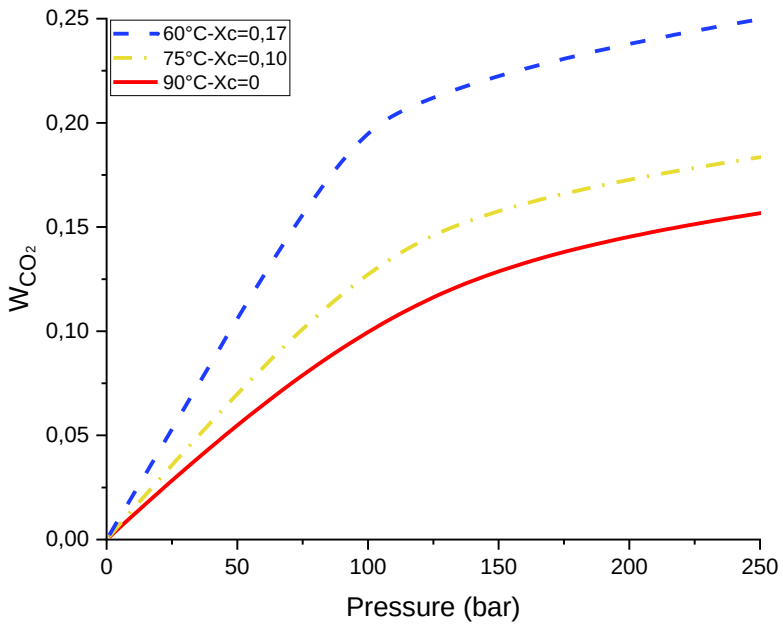

Figure 10: CO_2 mass fraction absorbed into EVA at equilibrium according to SL-EoS for different temperatures (60°C, 75°C and 90°C)

Therefore, a lower temperature (60°C), even considering the melting, is favourable to the absorption of a greater quantity of CO_2 within the EVA, about twice as much at 60°C as at 90°C for the pressures higher than 100 bar. For 75°C, the CO_2 mass fraction absorbed within EVA is intermediate but closer to the 90°C plot. In addition, the good correlation of the SL EoS with the experiment can be used to extrapolate data in pressure and temperature with an incertitude about the crystallinity in the melting range. As described in paragraph 1, the thermodynamic equilibrium is one aspect of the CO_2 absorption within a polymer, but absorption kinetics is also important for estimation of the necessary duration to treat a PV module with the aim to delaminate it. In addition, the swelling experiments can also be used to determine the diffusivity of CO_2 into EVA by considering the pressure change steps.

3.3. CO_2 absorption kinetic into EVA - Diffusivity

Swelling measurements by dynamic acquisition during pressure change steps allow the determination of the diffusion coefficient thanks to a fit from the mathematical crank solution for a “plane sheet" type geometric shape (8). Figure 11 shows examples of Crank’s plane sheet geometry fit at 75°C for different pressures. On Figure 11, the pressure-dependent change of slope is visible.

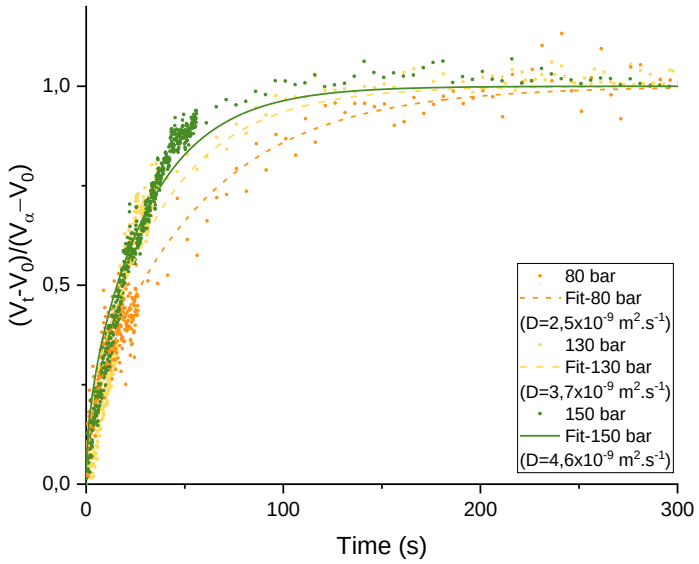

Figure 11: Examples of Crank's plane sheet geometry fit at 75°C for 80 bar, 130 bar and 150 bar. Each point represents one capture.

Using this method, the diffusion coefficient of CO_2 in EVA was determined as a function of pressure and temperature (Figure 12).

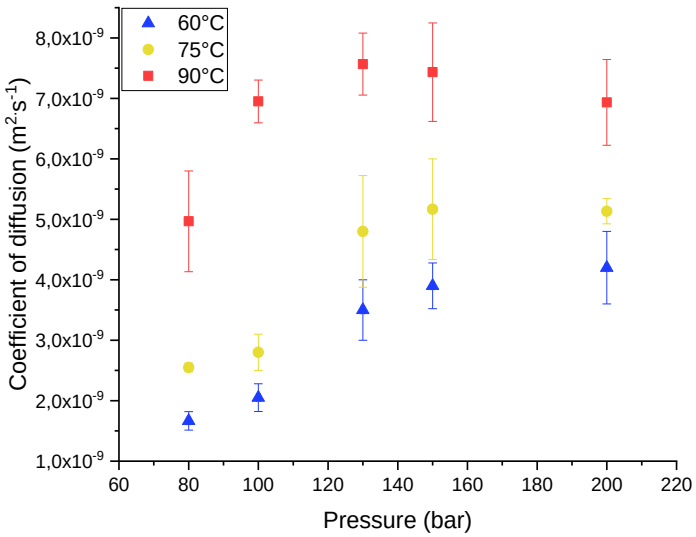

Figure 12: Coefficient of diffusion of CO_2 absorption into EVA in function of pressure for different temperatures: 60°C, 75°C and 90°C

The diffusion coefficient of CO_2 within the EVA increases with the pressure for each temperature. At 60°C and 75°C, the diffusion coefficient increases significantly between 100 bar and 130 bar. For 90°C, a clear increase of the diffusion coefficient occurs at a lower pressure, between 80 bar and 100 bar. From 130 bar onwards, the diffusion coefficient stabilises for the three temperatures under consideration. At 60°C the diffusion coefficient stabilises at about $4x10^{-9}$ m^2.s^{-1}; at 75°C, $5x10^{-9}$ m^2.s^{-1} and at 90°C, $7x10^{-9}$ m^2.s^{-1}. Consequently, the increase in temperature increases significantly the kinetics of CO_2 absorption within the EVA. These values are intermediates between the diffusion coefficient determined at 50°C

and 150 bar for an EVA-40 by swelling measurements [23] ($1x10^{-9}$ $m^2.s^{-1}$) and for another rubbery polymer PDMS, polymer for which CO_2 is known to be strongly diffusive, at 70°C and 150 bar [26] ($10x10^{-9}$ $m^2.s^{-1}$).

3.4. Photovoltaic module's interfaces influence on CO_2 diffusion into EVA

After studying CO_2 absorption within EVA alone, it is necessary to study the impact of the interfaces of a photovoltaic module on absorption, in particular diffusion. Indeed, knowledge of absorption within EVA alone is not sufficient to determine the processing time required for a photovoltaic module to be delaminated. For this purpose, the study of the interface diffusion for each of the interfaces in isolation (backsheet, rear face of the cell, front face of the cell and glass) provides elements of interest. Figure 13 shows the determination of interface diffusion coefficient at 150 bar and 75°C according to the protocol described in paragraph 2.6.

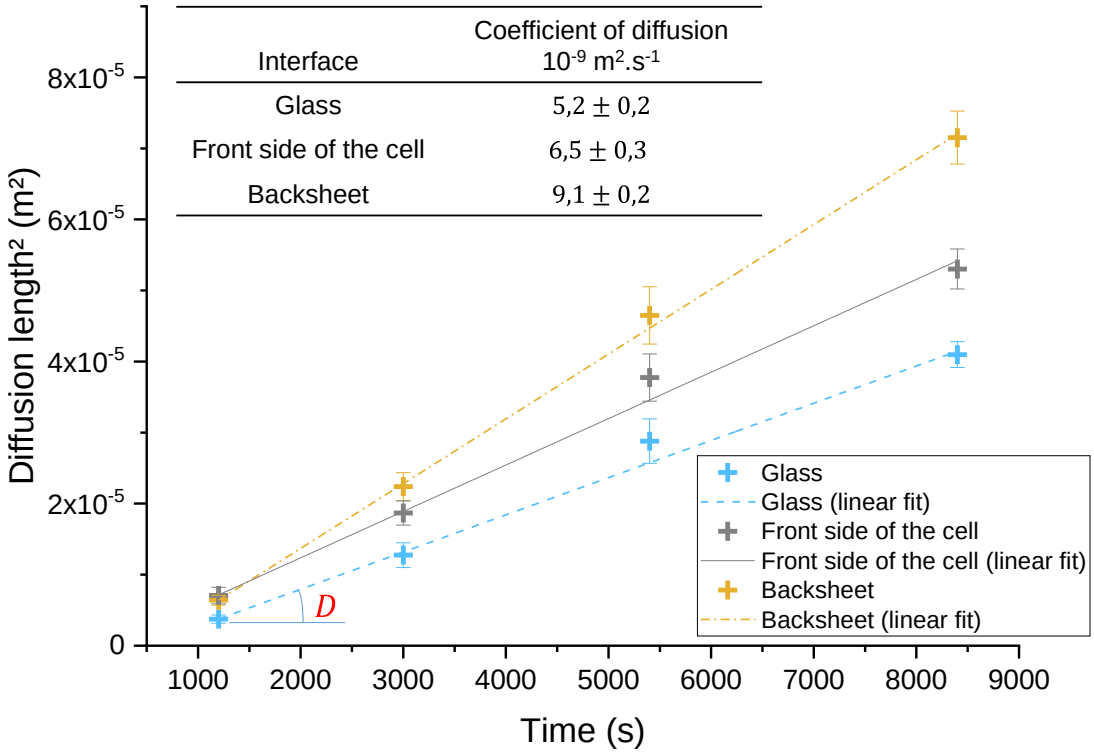

Figure 13 : Diffusion length measurements (+) and linear fit in function of time at 75°C and 150 bar for different PV module's interfaces (glass, front side of the cell and backsheet)

The interface diffusion coefficient for the glass interface ($5,2x10^{-9}$ $m^2.s^{-1}$) is similar to the diffusion coefficient determined for EVA at 150 bar and 75°C ($5,0x10^{-9}$ $m^2.s^{-1}$) but lower than that for other interfaces. It seems that for the glass, the contribution of the interface to the interface diffusion is almost null and the diffusion is mainly driven by the diffusivity of the CO_2 in EVA. However, for other cases the contribution of the interface on diffusion coefficient is not negligible, especially for the "backsheet" ($9,1x10^{-9}$ $m^2.s^{-1}$ at 150 bar and 75°C). This favourable contribution from the backsheet interface is probably due to specific favourable interactions between SC-CO_2 and fluor contained in PVF (layer of the "backsheet" in adhesion with EVA). Indeed, preferential interactions between SC-CO_2 and fluorinated components have been reported in literature ([34], [35]). Moreover, the interface diffusion in the rear side of the cell is not plotted in Figure 13. Indeed, a largely preferential diffusion was observed at this interface and did not allow any measurement of the interface diffusion length because even for the shortest measurement time (20 min) the CO_2 had diffused over the whole sample (for samples of 2cm x 5cm and even for samples of 10cm x 10cm). SEM's characterisation of the surface of this interface has made it possible to explain this preferential diffusion (Figure 14).

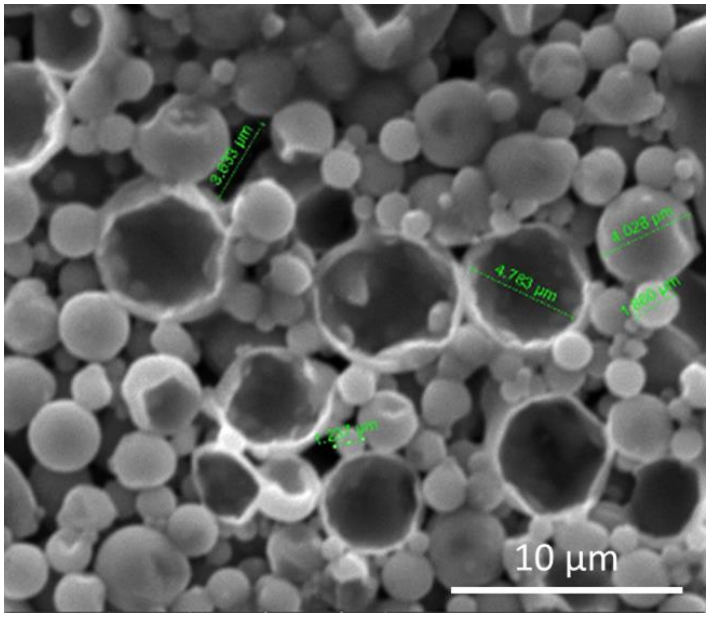

Figure 14: SEM micrograph of the rear side of the cell (x10 000)

Figure 14 shows an important porosity, of the order of the µm, in the rear side of the cell. The rear side of the Si-Al-BSF type photovoltaic cells is made of screen-printed aluminium. After annealing, this manufacturing process produces a microporous structure in the form of micrometric beads. This porous microstructure enables a preferential CO_2 diffusion at this interface.

4. Conclusion

This paper shows a global method to study the SC-CO_2 absorption into a polymer in a multilayer structure, in this particular case of the EVA in photovoltaic modules. Firstly, the EVA-28 characterization by HP-DSC allowed to determine the phase diagram of the polymer in CO_2 medium for pressures ranging from atmospheric pressure to 150 bar. These measurements demonstrated a low impact on the melting temperature of EVA, about a decrease of 7°C for the melting end from 60 bar.

Then, Sanchez-Lacombe EoS modified to take into account the crystallinity and the cross-linking of the EVA-28 showed a good correlation with the results obtained from the swelling experiments. This model can predict the quantity of CO_2 absorbed in the polymer for various operating pressures and temperatures which is an important information to describe the EVA foaming with the aim to delaminate a PV module.

In addition, the diffusion coefficient was determined thanks to swelling experiments. The results show that increasing temperature induces a significantly increase of CO_2 diffusivity into the EVA. The diffusion coefficient stabilizes at 130 bar, from $4x10^{-9}$ $m^2.s^{-1}$ (60°C); to$7x10^{-9}$ $m^2.s$ (90°C).

Finally, the impact of PV modules interfaces on the diffusion was studied by an original method of apparent length of diffusion post treatment. This study demonstrates a largely preferential diffusion at the rear side of the cell due to an important porosity of this interface. Moreover, a preferential diffusion was observed at the backsheet interface ($9x10^{-9}$ $m^2.s^{-1}$ at 150 bar and 75°C), probably due to the specific favourable interactions between SC-CO_2 and fluor contained in PVF (layer of the "backsheet" in adhesion with EVA). For other interfaces materials, the glass and the front side of the cell, the impact of the interfaces on the diffusion coefficient is lower. The data determined by this investigation on the SC-CO_2 absorption into the EVA in photovoltaic modules allows to estimate the processing times required for photovoltaic panels for delamination.

References

[1] ITRPV, « International Technology Roadmap for Photovoltaic (ITRPV) - Results of 2019 - 11th edition », 2020.

[2] I. IRENA, « End-Of-Life Management: Solar Photovoltaic Panels », *International Renewable Energy Agency and the International Energy Agency Photovoltaic Power Systems*, 2016.

[3] ITRPV, « International Technology Roadmap for Photovoltaic - Results 2016 », 8th Edition, 2017.

[4] C. E. L. Latunussa, F. Ardente, G. A. Blengini, et L. Mancini, « Life Cycle Assessment of an innovative recycling process for crystalline silicon photovoltaic panels », *Solar Energy Materials and Solar Cells*, vol. 156, p. 101-111, nov. 2016, doi: 10.1016/j.solmat.2016.03.020.

[5] V. Fiandra, L. Sannino, C. Andreozzi, et G. Graditi, « End-of-life of silicon PV panels: A sustainable materials recovery process », *Waste Management*, vol. 84, p. 91-101, 2019, doi: 10.1016/j.wasman.2018.11.035.

[6] A. Kuczyńska-Łazewska et E. Klugmann-Radziemska, « Influence of fragment size on the time and temperature of ethylene vinyl acetate lamination decomposition in the photovoltaic module recycling process », *Materials*, vol. 12, nº 18, 2019, doi: 10.3390/ma12182857.

[7] Y. Kim et J. Lee, « Dissolution of ethylene vinyl acetate in crystalline silicon PV modules using ultrasonic irradiation and organic solvent », *Solar Energy Materials and Solar Cells*, vol. 98, p. 317–322, mars 2012, doi: 10.1016/j.solmat.2011.11.022.

[8] W. S. Chen, Y. J. Chen, et Y. A. Chen, « The application of organic solvents and thermal process for eliminating EVA resin layer from waste photovoltaic modules », 2019, vol. 291, doi: 10.1088/1755-1315/291/1/012012.

[9] S. Kang, S. Yoo, J. Lee, B. Boo, et H. Ryu, « Experimental investigations for recycling of silicon and glass from waste photovoltaic modules », *Renewable Energy*, vol. 47, p. 152-159, 2012, doi: 10.1016/j.renene.2012.04.030.

[10] V. Savvilotidou et E. Gidarakos, « Pre-concentration and recovery of silver and indium from crystalline silicon and copper indium selenide photovoltaic panels », *Journal of Cleaner Production*, vol. 250, 2020, doi: 10.1016/j.jclepro.2019.119440.

[11] Y. K. Yi, H. S. Kim, T. Tran, S. K. Hong, et M. J. Kim, « Recovering valuable metals from recycled photovoltaic modules », *Journal of the Air & Waste Management Association*, vol. 64, nº 7, p. 797-807, juill. 2014, doi: 10.1080/10962247.2014.891540.

[12] S. Syed, « Silver recovery aqueous techniques from diverse sources: Hydrometallurgy in recycling », *Waste Management*, nº 50, p. 234-256, 2016.

[13] S.-Y. Cho, T.-Y. Kim, et P.-P. Sun, « Recovery of silver from leachate of silicon solar cells by solvent extraction with TOPO », *Separation and Purification Technology*, vol. 215, p. 516-520, 2019.

[14] F. Ardente, C. E. L. Latunussa, et G. A. Blengini, « Resource efficient recovery of critical and precious metals from waste silicon PV panel recycling », *Waste Management*, vol. 91, mai 2019, doi: 10.1016/j.wasman.2019.04.059.

[15] J. Shin, J. Park, et N. Park, « A method to recycle silicon wafer from end-of-life photovoltaic module and solar panels by using recycled silicon wafers », *Solar Energy Materials and Solar Cells*, vol. 162, p. 1-6, 2017, doi: 10.1016/j.solmat.2016.12.038.

[16] J. L. Sumey, J. A. Sarver, et E. Kiran, « Foaming of polystyrene and poly(methyl methacrylate) multilayered thin films with supercritical carbon dioxide », *Journal of Supercritical Fluids*, vol. 145, p. 243-252, 2019, doi: 10.1016/j.supflu.2018.12.001.

[17] S. Sanyal *et al.*, « Understanding and optimizing delamination/recycling of printed circuit boards using a supercritical carbon dioxide process », *Journal of Cleaner Production*, vol. 41, p. 174-178, 2013, doi: 10.1016/j.jclepro.2012.10.011.

[18] D. L. Tomasko *et al.*, « A Review of CO2 Applications in the Processing of Polymers », *Ind. Eng. Chem. Res.*, vol. 42, nº 25, p. 6431-6456, déc. 2003, doi: 10.1021/ie030199z.

[19] Z. Chen, K. Cao, Z. Yao, et Z. Huang, « Modeling solubilities of subcritical and supercritical fluids in polymers with cubic and non-cubic equations of state », *The Journal of Supercritical Fluids*, vol. 49, nº 2, p. 143-153, juin 2009, doi: 10.1016/j.supflu.2008.12.013.

[20] J. K. Lee, S. X. Yao, G. Li, M. B. G. Jun, et P. C. Lee, *Measurement Methods for Solubility and Diffusivity of Gases and Supercritical Fluids in Polymers and Its Applications*, vol. 57. 2017.

[21] G. Mensitieri, G. Scherillo, C. Panayiotou, et P. Musto, « Towards a predictive thermodynamic description of sorption processes in polymers: The synergy between theoretical EoS models and vibrational spectroscopy », *Materials Science and Engineering R: Reports*, vol. 140, 2020, doi: 10.1016/j.mser.2019.100525.
[22] Y.-T. Shieh et Y.-G. Lin, « Equilibrium solubility of CO2 in rubbery EVA over a wide pressure range: Effects of carbonyl group content and crystallinity », *Polymer*, vol. 43, nº 6, p. 1849-1856, 2002, doi: 10.1016/S0032-3861(01)00776-5.
[23] M. A. Jacobs, F. K. Maartje, et J. T. F. Keurentjes, « Foam processing of poly(ethylene-co-vinyl acetate) rubber using supercritical carbon dioxide », *Polymer*, 2004.
[24] S. Ogier, « Etude et optimisation de procédés d'encapsulation de cellules photovoltaïques », Université de Lorraine, Metz, 2017.
[25] E. Huang, X. Liao, C. Zhao, C. B. Park, Q. Yang, et G. Li, « Effect of Unexpected CO2's Phase Transition on the High-Pressure Differential Scanning Calorimetry Performance of Various Polymers », *ACS Sustainable Chemistry and Engineering*, vol. 4, nº 3, p. 1810-1818, 2016, doi: 10.1021/acssuschemeng.6b00008.
[26] J. R. Royer, J. M. DeSimone, et S. A. Khan, « Carbon dioxide-induced swelling of poly(dimethylsiloxane) », *Macromolecules*, vol. 32, nº 26, p. 8965-8973, 1999, doi: 10.1021/ma9904518.
[27] I. C. Sanchez et R. H. Lacombe, « Statistical Thermodynamics of Polymer Solutions », *Macromolecules*, vol. 11, nº 6, p. 1145-1156, nov. 1978, doi: 10.1021/ma60066a017.
[28] M. B. Kiszka, M. A. Meilchen, et M. A. McHugh, « Modeling high-pressure gas–polymer mixtures using the sanchez-lacombe equation of state », *Journal of Applied Polymer Science*, vol. 36, nº 3, p. 583-597, 1988, doi: 10.1002/app.1988.070360311.
[29] F. Doghieri et G. C. Sarti, « Nonequilibrium Lattice Fluids: A Predictive Model for the Solubility in Glassy Polymers », *Macromolecules*, vol. 29, nº 24, p. 7885-7896, janv. 1996, doi: 10.1021/ma951366c.
[30] C. Panayiotou et I. C. Sanchez, « Swelling of network structures », *Polymer*, vol. 33, nº 23, p. 5090-5093, 1992, doi: 10.1016/0032-3861(92)90064-4.
[31] M. Minelli et M. G. De Angelis, « An equation of state (EoS) based model for the fluid solubility in semicrystalline polymers », *Fluid Phase Equilibria*, vol. 367, p. 173-181, 2014, doi: 10.1016/j.fluid.2014.01.024.
[32] J. Crank, *The Mathematics of Diffusion, Second Edition*. Brunel University Uxbridge, 1975.
[33] J. A. Sarver, J. L. Sumey, M. L. Williams, J. P. Bishop, D. M. Dean, et E. Kiran, « Foaming of poly(ethylene-co-vinyl acetate) and poly(ethylene-co-vinyl acetate-co-carbon monoxide) and their blends with carbon dioxide », *Journal of Applied Polymer Science*, vol. 135, nº 7, p. 45841, févr. 2018, doi: 10.1002/app.45841.
[34] Y. Kachi, T. Tsukahara, Y. Kayaki, T. Ikariya, J. Sato, et Y. Ikeda, *Raman spectral shifts of CO2 as measure of CO2-philicity of solutes in supercritical carbon dioxide*, vol. 40. 2007.
[35] A. V. Yazdi et E. J. Beckman, « Design of Highly CO2-Soluble Chelating Agents. 2. Effect of Chelate Structure and Process Parameters on Extraction Efficiency », *Ind. Eng. Chem. Res.*, vol. 36, nº 6, p. 2368-2374, juin 1997, doi: 10.1021/ie960611t.